



Design, synthesis, biological evaluation and molecular dynamics simulation studies of (R)-5-methylthiazolidin-4-one derivatives as megakaryocyte protein tyrosine phosphatase 2 (PTP-MEG2) inhibitors for the treatment of type 2 diabetes

Jingwei Wu, Yingzhan Sun, Hui Zhou, Ying Ma & Runling Wang

To cite this article: Jingwei Wu, Yingzhan Sun, Hui Zhou, Ying Ma & Runling Wang (2019): Design, synthesis, biological evaluation and molecular dynamics simulation studies of (R)-5-methylthiazolidin-4-one derivatives as megakaryocyte protein tyrosine phosphatase 2 (PTP-MEG2) inhibitors for the treatment of type 2 diabetes, Journal of Biomolecular Structure and Dynamics, DOI: [10.1080/07391102.2019.1654410](https://doi.org/10.1080/07391102.2019.1654410)

To link to this article: <https://doi.org/10.1080/07391102.2019.1654410>



Accepted author version posted online: 11 Aug 2019.



Submit your article to this journal [↗](#)



View Crossmark data [↗](#)

Design, synthesis, biological evaluation and
molecular dynamics simulation studies of (R)-5-
methylthiazolidin-4-one derivatives as
megakaryocyte protein tyrosine phosphatase 2 (PTP-
MEG2) inhibitors for the treatment of type 2
diabetes

Jingwei Wu^{a, ‡}, Yingzhan Sun^{a, ‡}, Hui Zhou^a, Ying Ma^{a, *}, Runling Wang^{a, *}

^aTianjin Key Laboratory on Technologies Enabling Development of Clinical Therapeutics and
Diagnostics (Theranostics), School of Pharmacy, Tianjin Medical University, Tianjin 300070,
China

[‡] These authors contributed equally to this work

*Corresponding authors: Ying Ma, E-mail: maying@tmu.edu.cn

Runling Wang , E-mail:wangrunling@tmu.edu.cn

Keywords: PTP-MEG2; type 2 diabetes; De novo design; synthesis; molecular dynamics simulation

Abstract

PTP-MEG2 plays a significant role in insulin production and is able to enhance insulin signaling and improve insulin sensitivity. So, PTP-MEG2 inhibitors are closely associated with type 2 diabetes therapy. A series of novel (R)-5-methylthiazolidin-4-one derivatives were designed and synthesized, and their PTP-MEG2 inhibitory activities (IC_{50}) were determined. Among the desired compounds, **1h** shares the highest inhibitory activity ($IC_{50} = 1.34 \mu M$) against PTP-MEG2. Additionally, various post-dynamic analyses confirmed that when compound **1h** bound to the PTP-MEG2, the protein conformations became unstable and the function of the pTyr recognition loop (Asn331-Cys338) would be disturbed. And thus, the ideal conformations needed for the catalytic activity was difficult to be maintained. In brief, these might be how the compound **1h** worked. Furthermore, we also found that the key residues Arg332 would play a critical role in disturbing the residue interactions.

List of abbreviations

DCCM (dynamic cross-correlation mapping); DMF (N,N-dimethylformamide); DSSP (definition of secondary structure of proteins); FOXO (forkhead transcription factors); MD (molecular dynamics); PCA (principal component analysis); PDB (protein data bank); PTKs (protein tyrosine kinases); PTPs (protein tyrosine phosphatases); PTP-MEG2 (megakaryocyte protein

tyrosine phosphatase 2); RIN (residue interaction network); RING (Residue Interaction Network Generator); RMSD (root means square deviation); RMSF (root mean square fluctuation);

1 Introduction

Protein tyrosine phosphatases (PTPs) comprise a superfamily of signaling enzymes which are important in lots of cellular processes, such as cell proliferation, differentiation, migration, adhesion and apoptosis(Hendriks et al. 2013; Lee, Yi, Lawan, Min & Bennett 2015). PTPs are catalyzed by protein tyrosine kinases (PTKs), which are vital for proper level of cellular protein tyrosyl phosphorylation. Alterations in PTP genes contribute to human diseases, including cancer or metabolic disorders(He, Zeng, He, Zhang & Zhang 2013; Hendriks, Bourgonje, Leenders & Pulido 2018). Therefore, PTPs are promising drug targets(Zhang 2001).

The non-receptor PTP-MEG2 (also namedPTPN9)(Wang et al. 2019) is the unique mammalian representative of PTPs, which is highly expressed at highest levels in leukocytes, brain, exocrine and endocrine cells(Qi et al. 2002; Huynh et al. 2003). It has been proved that PTP-MEG2 is a regulator of insulin-dependent FOXO1 subcellular localization and controls insulin signaling and insulin production (Cho et al. 2006; Gurzov, Stanley, Brodnicki & Thomas 2015; Chatterjee, Khunti & Davies 2017). Indeed, treatment with PTP-MEG2 inhibitors can enhance insulin action both *in vivo* and *in vitro*, indicating that PTP-MEG2 may be an effective therapeutic target of type 2 diabetes(Cho et al. 2006).

The PTP catalytic site (i.e., pTyr) alone is not sufficient for high-affinity binding while the adjacent residues are also conducive to PTP substrate recognition. Reports have showed that there are neighbouring sub-pockets, which can be targeted for PTP-MEG2 inhibitors(Zhang et al. 2009). Inspired by these discoveries, we design a series of PTP-MEG2 inhibitors by means of

fragment-based de novo design involving virtual screening, molecular docking and molecular dynamics simulation., In order to discover some potential PTP-MEG2 inhibitors for the treatment of type 2 diabetes, a series of thiazolidin-4-one derivatives were synthesized and their PTP-MEG2 inhibitory activities (IC_{50}) were determined. In the meantime, molecular dynamics simulations could provide the fundamental information concerning individual particle motions over time. Therefore, the application of the 100 ns MD molecular dynamics could explore the effect of **1h** on the PTP-MEG2, and various post-analyses were carried out to analyze the mechanisms of inhibition at the molecular level. The root means square deviation (RMSD) firstly verified the PTP-MEG2 and PTP-MEG2/**1h** systems were stable and available. The root mean square fluctuation (RMSF) and radius of gyration (Rg) analyses showed that the protein conformation became unstable and the fluctuation of the the pTyr recognition loop (Asn331-Cys338) was decreased in the PTP-MEG2/**1h** system. The Dynamics cross-correlation matrix analysis (DCCM) results and principal component analysis (PCA) had similar results with the above Rg and RMSF analyses, which further verified that when inhibitor **1h** bound to the protein, the PTP-MEG2 owned unstable conformation and the pTyr recognition loop had low flexibility. The study on the residue interaction network (RIN) revealed that the key residues Arg332, played an important role in breaking the residue interactions in the PTP-MEG2/**1h** system. In brief, the inhibitor owned large inhibitor effect for the PTP-MEG2 in this study.

2 Material and Methods

Our calculations were carried out on Dell Precision TM T5500 computer with Discovery Studio 3.5 software package (<http://accelrys.com/>).

2.1 Compound design

2.1.1 Virtual screening

Virtual screening has become an effective method for the lead discovery and optimization. (Shoichet 2004; Li et al. 2009; Liu et al. 2011). In the present study, docking-based virtual screening was performed using LibDock (Accelrys Discovery Studio package), because it has been applied to the GSK validation data set (Diller & Merz 2001).

The receptor crystal structure of catalytic domain of PTP-MEG2 (PDB ID:4GE6) (Zhang et al. 2009) was downloaded from the protein data bank (PDB) (Berman et al. 2002) and was used for molecular docking. The ligands utilized for virtual screening were retrieved from Drugs-Now database and Drugs-Like in ZINC database (Irwin & Shoichet 2005). The preparation for all compounds and the protein were performed by the Prepare Ligands and Prepare Protein protocols, respectively. The binding sites sphere was defined using “Find Site From Current Selection” based on the key residues in the catalytic pocket (The pTyr recognition loop, residues 331–338) and the sub-pocket (residues 514–521, residues 558–564) (Zhang et al. 2009). All investigated ligands from ZINC database were docked to the binding pocket with the method of LibDock. According to the docking scores, the best candidate was identified as potential scaffold used for the following study of De Novo Design.

2.1.2 De Novo Design

The technology of “De novo design” has been often used in the design of drug candidates for lots of pharmaceutically relevant targets (Loving, Alberts & Sherman 2010). The flowchart showing the process of De novo design was illustrated in **Figure 1**. The protocol of “De Novo Library Generation” was used to create fragment library, which was used in the following step “De Novo Evolution”. In view of pharmacological activity, the fragments were retrieved from drugs-now

database. The protocol of De Novo Evolution could develop the new derivatives in the binding pocket environment of the receptor based on the scaffold native structure. The Ludi algorithm(Böhm 1992) was used to fit appropriate fragments to scaffold obtained by virtual screening, and then produced a collection of the new derivatives with higher scores(Law et al. 2009). The evolution mode was set to full evolution, which allows the scaffold to link up to a maximum of three fragments. The maximum number of survivors, population size and generations were set to 2, 10 and 2, respectively(Wu et al. 2014). Finally, top-ranked “LibDock SCORE” molecules were selected for the following chemical synthesis.

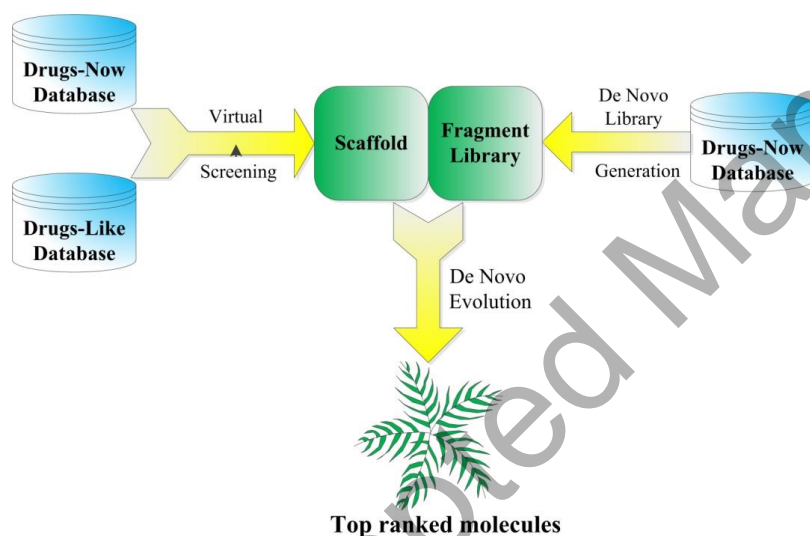
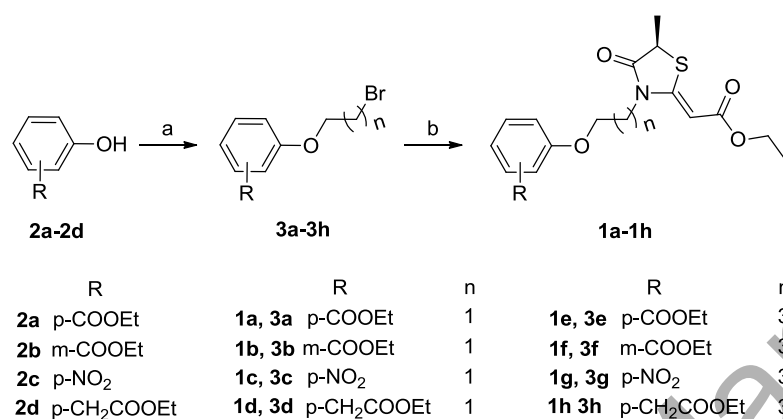


Figure 1. The de novo design flowchart. The database and the methods used for de novo design were depicted as blue cylinder and yellow arrows, respectively.

2.2 Chemistry

Melting points were measured with an RY-2 microscopic melting point apparatus and are uncorrected. ^1H NMR and ^{13}C NMR spectra were recorded on a Bruker AV400 NMR spectrometer with CDCl_3 or DMSO-d_6 as solvent and known chemical shifts of residual proton

signals of deuterated solvents (^1H NMR: 7.26 ppm for CDCl_3) or carbon signals of deuterated solvents (^{13}C NMR: 39.52 ppm for DMSO-d_6) as internal standard. MS spectra were obtained with an Agilent Q-TOF 6510 mass spectrometer with electro-spray ionization technique (in ESI+/ESI- mode) using direct injection method. The synthetic route to the desired products **1a-1h** is illustrated in **Schemes 1**. For synthetic details, see the supporting information.



Scheme 1 Synthetic routes to desired products **1a-1h**

Reagents and conditions: a. 1,2-dibromoethane (for **3a-3d**) or 1,4-dibromobutane (for **3e-3h**), aq. K_2CO_3 , EtOH/ H_2O (v/v = 1:1), 80 °C; b. (R,Z)-ethyl 2-(5-methyl-4-oxothiazolidin-2-ylidene)acetate, KI, K_2CO_3 , DMF, r.t.

2.3 Enzymatic assays

The activity of PTP-MEG2 was assessed at 37 °C in 96-well plates with p-nitrophenyl phosphate (pNPP) as substrate. Purified recombinant PTP-MEG2 (0.1 μg) in 60 μL buffer with 60 mM calcium citrate, 2 mM EDTA, and 2 mM dithiothreitol and each sample were added to each well of a 96-well plate. After preincubation for 2 min at 37°C, 50 μL of buffer with 40 μL pNPP was added and incubated. After incubation for 30 min, the reaction was quenched by adding 10 μL of

a 0.2 N NaOH solution, and the absorbance at 405 nm was measured. IC₅₀ values were determined as the concentration of compounds that gave 50% of the control enzyme activity.

2.4 Molecular Dynamics Simulations

2.4.1 System preparation

The X-ray crystal structure of PTP-MEG2 (PDB ID: 4GE6) was derived from the Protein Data Bank (PDB) and prepared by the “prepare protein” in DS v3.5 (Ma, Wang, Xu, Wang & Chou 2012). The process of the “prepare protein” included the following steps: firstly, the H₂O in the protein was removed; secondly, the intramolecular bond orders were assigned; thirdly, the hydrogen atoms were added to the structure; and then, the disulfides and metals in protein were treated; finally, Modeler (Chimera) was used to add the missing residues (Cheng et al. 2012; Zhang, Wang, Xu, Wang & Wang 2012). The structure of the PTP-MEG2 was crystallized as a dimer; only chain A was considered for the simulations, therefore, the chain B was deleted. And then, the molecular dynamic simulations were carried out.

2.4.2 Molecular Dynamics Simulations

Conventional MD simulations in the study were performed to assess the effect of complex **1h**. Both PTP-MEG2 and PTP-MEG2/**1h** systems were performed to run 100 ns MD simulations (Fakhar et al. 2017; Li et al. 2018). With the help of the single-point charge (SPC) water model (MacKerell et al. 1998) and periodic boundary conditions, the two proteins were solvated in dodecahedral 1.0 nm, respectively. The PTP-MEG2 system was solvated in about 3547 SPC water molecules and the PTP-MEG2/**1h** system was solvated in about 3552 SPC water molecules. To neutralize the positive charge in the two systems, three chlorine (3 Cl⁻ ions)

counter ions were added to replace the solvent molecules randomly. In the process of the minimization, there were 50,000 steps in the simulations to perform steepest descent energy minimization until the maximum force was less than 10.0 KJ/mol (Berhanu & Masunov 2014). Afterwards, the temperature and pressure of the two systems were stable at 310 K and 1 bar under the 100 ps NVT and NPT simulation conditions, respectively (Foster & West 2017). Meanwhile, the particle-mesh Ewald algorithm was utilized to manage the long-range electrostatic interactions, and bond lengths were constrained at their equilibrium values by the LINCS algorithm (Li et al. 2018). The two systems were performed 100 ns molecular dynamics simulations, respectively. The trajectories were stored in the traj.trr file for the two models at every 20 ps, and structural analysis was done at every picosecond. Post dynamics analysis were carried out to compare the two models to find out the effect of the compound **1h** on the PTP-MEG2, including the RMSD, Rg, RMSF, PCA, DCCM and RIN analyses.

2.4.3 Principal component analysis

PCA has been utilized to give a deep insight of the dynamics of a protein system (Sittel, Jain & Stock 2014). In this study, PCA was carried out on C α atoms on 1000 snapshots extracted from 8~100 ns MD trajectories. The conformational changes of proteins and the atomic displacement in a collective manner can be defined using PCA (Buslaev, Gordeliy, Grudinin & Gushchin 2016). The correlated motions of whole protein can be represented by the eigenvectors and eigenvalues. Therefore, the PC1, PC2 and PC3 (first three principal components) were computed, which contributed more significantly in PCA analysis. The PCA method could be calculated by the following formula (Balmith & Soliman 2017):

$$C_{ij} = \langle (X_i - \langle X_i \rangle) (X_j - \langle X_j \rangle) \rangle (i, j = 1, 2, 3 \dots, 3N)$$

Where, the i/j -th alpha carbon atoms are represented by the $X_{i/j}$, the time average is represented by the $\langle X_{i/j} \rangle$ and N is considered as the number of C_α atoms. The tool of the Bio3D library in the R and ProDy software are utilized to carry out the analysis.

2.4.4 Dynamics cross-correlation matrix analysis

To gather a deeper insight of the dynamics of PTP-MEG2 and PTP-MEG2/1h structures, the DCCM was used to determine cross-correlated displacements of backbone alpha carbon atoms in the molecular dynamic trajectories for the two systems, and was analyzed by the following formula(Lukman, Lane & Verma 2013):

$$C_{ij} = \frac{(\Delta r_i \times \Delta r_j)}{(\langle \Delta r_i^2 \rangle \langle \Delta r_j^2 \rangle)^{1/2}}$$

Here, i/j corresponds to i/j -th residues and $\Delta r_{i/j}$ represents the displacement of i/j -th atoms from the mean, respectively. This analysis was also performed by the Bio3D library in the R and ProDy software(Aier, Varadwaj & Raj 2016).

2.4.5 Residue interaction networks analysis

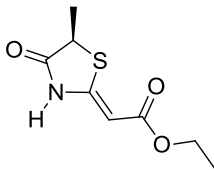
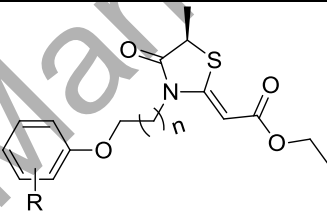
RIN analysis could show the detailed interactions between residues in protein(Niu et al. 2017), which was an alternative way of representing protein structures and has been utilized for analyzing the structural changes of protein interaction network with inhibitor, protein folding and catalytic activity. In the RINs, the edges represented the interactions between pairs of residues and the nodes represented residues of a protein. According to the type of interaction, the edges were labeled as van der Waal, salt bridges and hydrogen bonds interactions, respectively. The Cytoscape network file for the PTP-MEG2 and PTP-MEG2/ inhibitor systems could be

constructed by the RING v2.0.1(Piovesan, Minervini & Tosatto 2016). The Cytoscape 3.6.1(Shannon et al. 2003) was utilized to constructed the RINs, using the Cytoscape network file. The tool of RINalyzer in Cytoscape 3.6.1 was used to observe the network. The closeness centrality, shortest path betweenness and the degree of residues could be calculated by the tool of RINalyzer and NetworkAnalyzer in the Cytoscape.

3. Results and discussion

3.1 Compounds design

Table 1. Structure and PTP-MEG2 inhibitory activity of compounds **1a-1h** and ZINC5852926

<div style="display: flex; align-items: center; justify-content: space-around;"> <div style="text-align: center;">  <p>ZINC5852926</p> </div> <div style="text-align: center;"> <p>De Novo Evolution</p> <p>→</p> </div> <div style="text-align: center;">  <p>1a-1h</p> </div> </div>					
Compounds	R	n	MW	LibDock Score	IC ₅₀ (μM)
ZINC5852926	-	-	201.243	101.732	>50
1a	p-COOEt	1	393.45	129.736	8.41±0.51
1b	m-COOEt	1	393.45	135.991	7.82±0.46
1c	p-NO ₂	1	366.39	131.773	13.33±0.78

1d	p-CH ₂ COOEt	1	407.48	137.817	3.62±0.21
1e	p-COOEt	3	406.47	128.492	2.77±0.16
1f	m-COOEt	3	406.47	130.559	5.03±0.31
1g	p-NO ₂	3	394.44	132.410	7.54±0.45
1h	p-CH ₂ COOEt	3	435.53	136.556	1.34±0.08

Accepted Manuscript

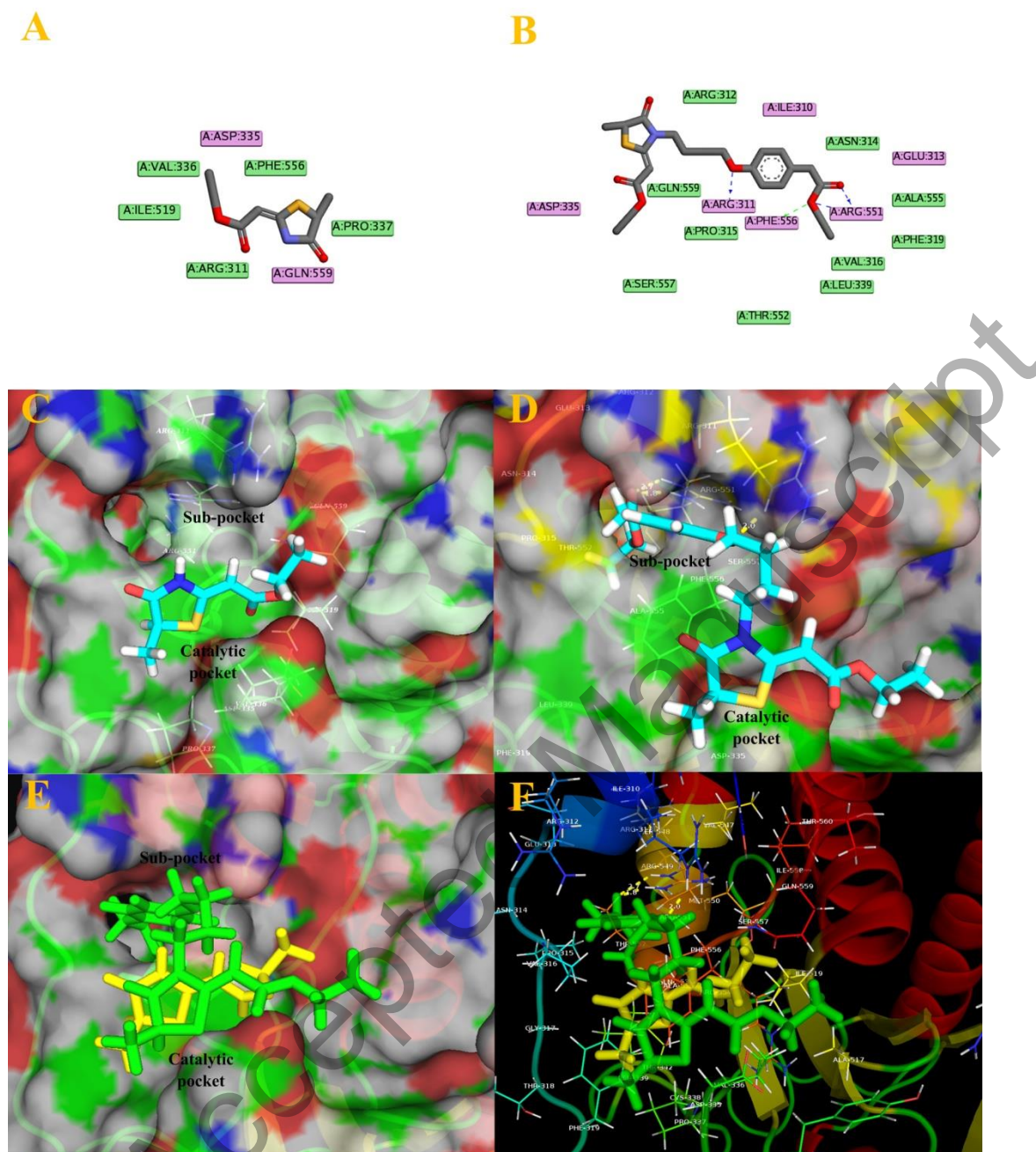


Figure 2. Structures and binding interactions of 4GE6 in complex with ZINC5852926 and compound **1h**. (A) 2D diagram of the interaction of ZINC5852926- PTP-MEG2. Residues involved in hydrogen-bond, charge or polar interactions are represented by pink boxes. Residues involved in van der waals interactions are represented by green boxes. (B) 2D diagram of the interaction of compound **1h**-PTP-MEG2. Hydrogen-bond interactions with amino acid main

chains and side chains are represented by a green and blue dashed arrow directed towards the electron donor. (C) The docked pose of ZINC5852926 in the catalytic pocket of 4GE6. (D) The docked pose of compound **1h** in the catalytic pocket and the adjacent sub-pocket of PTP-MEG2. (E) The aligned pose of ZINC5852926 (yellow) and compound **1h** (green) in the active sites of 4GE6. (F) Surface representation of 4GE6 in complex with ZINC5852926 (yellow) and compound **1h** (green). Hydrogen bond interactions were depicted as yellow-dashed lines. The **Figures** were created using Discovery Studio 3.5 software package (<http://accelrys.com/>) and PyMol (<http://www.pymol.org>).

ZINC5852926, as the best scaffold, was discovered in the virtual screening procedure (**Figure 1**). The following de novo design led to the discovery of 8 novel compounds (**1a-1h**) by the protocol of “De Novo Evolution”. The properties and docking scores of 8 compounds (**1a-1h**) as well as the scaffold (ZINC5852926) were summarized in **Table 1**. The LibDock score is a measure of the strength of binding between the ligand and the receptor. The higher score indicates stronger binding interaction between them (Diller & Merz Jr 2001). Examination of the LibDock score (**Table 1**) revealed that the scores for those 8 compounds have exceeded that of the scaffold (ZINC5852926), signifying that these desired compounds (**1a-1h**) would bind to the PTP-MEG2 more strongly than the scaffold (ZINC5852926).

The 2D diagrams of ZINC5852926-PTP-MEG2 as well as compound **1h**- PTP-MEG2 were shown in **Figure 2A** and **Figure 2B**, respectively. Comparing with the **Figure 2A**, we could find more interactions formed between compound **1h**- PTP-MEG2 in **Figure 2B**, green boxes such as Arg312, Asn314, Pro315, Val316, Phe319, Leu339, Thr552, Ala555, Ser557 and Gln559 represented van der waals interactions, while pink boxes like Ile310, Arg311, Glu313, Asp335, Arg551 and Phe556 were involved in hydrogen bond interaction, polar or charge interaction.

Moreover, the oxygen atoms formed one potential H-bond with the main chain of Phe556 (green dashed arrow in **Figure 2B**) and three potential H-bond with the side chains of Arg311 and Arg551 (blue dashed arrow in **Figure 2B**). The docked conformations of ZINC5852926 and **1h** to PTP-MEG2 were showed in **Figure 2C**, **Figure 2D** and **Figure 2E**, respectively. Obviously, compounds **1h** (green, **Figure 2E**) occupied both of the catalytic pocket and the adjacent sub-pocket while ZINC5852926 (yellow, **Figure 2E**) could only bind the catalytic pocket. In addition, the binding surfaces of 4GE6 in complex with ZINC5852926 (yellow) and compound **1h** (green) were shown in **Figure 2F**, compound **1h** formed the important H-bond (depicted as yellow-dashed lines) in the sub-pocket. This may be able to explain why the compound **1h** inhibited the PTP-MEG2 with a lower IC_{50} than ZINC5852926.

3.2 Chemistry

Firstly, the synthetic route to desired products **1a-1h** was shown in **Scheme 1**. O-alkylation of phenol derivatives (**2a-2d**) with 1,2-dibromoethane (for **3a-3d**) or 1,4-dibromobutane (for **3e-3h**) in the presence of K_2CO_3 in EtOH/ H_2O at $80^\circ C$ smoothly afforded **3a-3h** according to known procedures (Zhang et al. 2017). Secondly, N-alkylation of (R,Z)-ethyl 2-(5-methyl-4-oxothiazolidin-2-ylidene)acetate with **3a-3h** in the presence of KI as catalyst and K_2CO_3 as base in DMF at room temperature produced the final desired products **1a-1h** (Wu et al. 2019).

3.3 In vitro PTP-MEG2 inhibitory activity

The results of *in vitro* inhibitory assay of 8 synthesized compounds (**1a-1h**) as well as scaffold ZINC5852926 against PTP-MEG2 are summarized in **Table 1**. It is very clear that all the desired compounds (**1a-1h**) showed significantly improved PTP-MEG2 inhibitory activity (IC_{50} values were range from $1.34\ \mu M$ to $13.33\ \mu M$) as compared with scaffold ZINC5852926 ($IC_{50} > 50\ \mu M$).

Besides, it was found that the PTP-MEG2 inhibitory activity slightly increased as the length of alkyl groups increased (**1a** < **1e**, **1b** < **1f**, **1c** < **1g**, **1d** < **1h**). Moreover, it should be noted that the best and the worst R group in the benzene ring was p-CH₂COOEt and p-NO₂, respectively (**1d** > **1b** > **1a** > **1c**, **1h** > **1e** > **1f** > **1g**). In summary, *in vitro* inhibitory assay of 8 synthesized compounds led to the discovery of a potent novel compound **1h** (IC₅₀ = 1.34 μM), which had more inhibitory activity than the scaffold ZINC5852926 .

3.4 Post-dynamics analyses

3.4.1 Root mean square deviation (RMSD)

It could be seen from the **Figure 3** that both the two systems reached equilibrium and stabilization from 8 ns simulation. This result illustrated that the 100 ns molecular dynamics simulations for the two systems were credible and available.

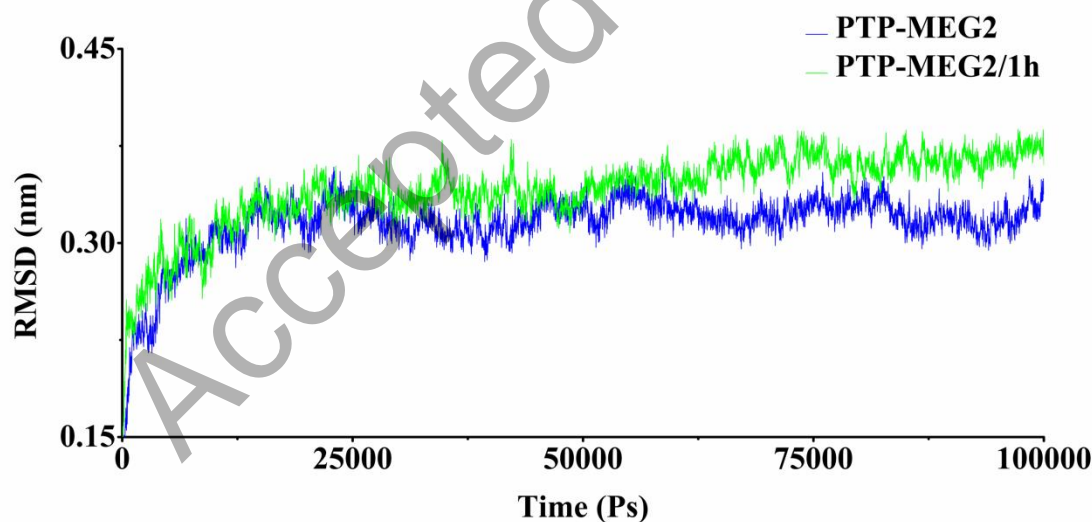


Figure 3 C α backbone RMSD for PTP-MEG2 system (blue line) and PTP-MEG2/**1h** system (green line) over a 100 ns MD simulation.

As shown in the **Figure 3**, the results indicated more flexible nature of residues in PTP-MEG2/**1h** system than that in PTP-MEG2 system. The results showed that the fluctuation of C α in the PTP-MEG2/**1h** system was increased, which could obviously show that the stability of conformations of PTP-MEG2/**1h** would be reduced.

3.4.2 Radius of gyration (Rg) and Root mean square fluctuation (RMSF) analyses.

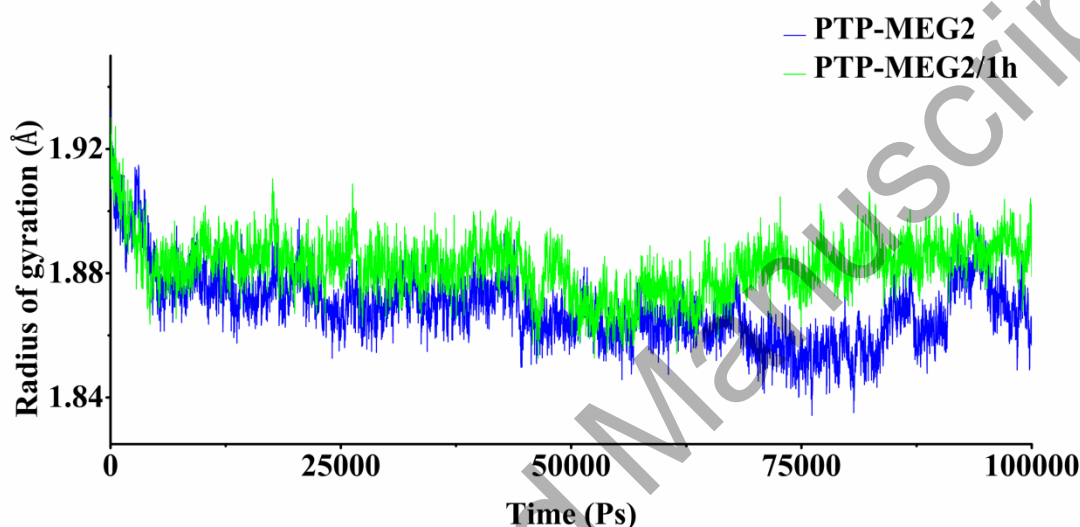


Figure 4 Rg comparison across the 100 ns MD simulation of the PTP-MEG2 system (blue line) and PTP-MEG2/**1h** system (green line).

As shown in the **Figure 4**, to provide further insight into the stability of biological molecules, as well as to determine the compactness of the tertiary structure of a protein throughout the MD simulation, Rg was calculated (Ndagi, Mhlongo & Soliman 2017). It could be seen from the **Figure** that the whole trend of the fluctuations of the two systems was similar compactness. However, we could still discover that the PTP-MEG2 system showed a lower average Rg of 1.86 Å than PTP-MEG2/**1h** system with an average Rg of 1.88 Å. The increase might reflect highly unstable nature of PTP-MEG2/**1h** system as compared to the PTP-MEG2 system. This was

agreed with the above RMSF and RMSD assumption that the compound **1h** decreased the interactions between the amino acids and the amino acids resulting in the changes of the conformational stability in the PTP-MEG2/**1h**.

The RMSF is a measure of the average atomic mobility of backbone atoms (N, C α and C) during MD simulation. As shown in the **Figure 5**, RMSF was monitored throughout the 100 ns molecular dynamics simulation. The function of a protein does not only depend on its structure but also on its dynamics. The function of a protein can be altered through interactions with the active site, or indirectly by disrupting motions essential to its function; more specifically, the essential motions induced by the conformational changes. It was obviously found that the fluctuations of three regions (Leu328-Asp335, Tyr366-Asn370 and Val495-Ser502) were reduced in the PTP-MEG2/**1h** system, with the average value 0.229 nm, 0.180 nm and 0.222 nm, respectively. In the PTP-MEG2 system, the average values of these regions were 0.314 nm, 0.272 nm and 0.337 nm, respectively. The differences of these regions between the PTP-MEG2 system and the PTP-MEG2/**1h** system were 0.085 nm, 0.092 nm and 0.115 nm. The results suggested that the compound **1h** had effect on the three regions with decreasing the interaction between the residues and residues. Interestingly, the conformations of residues of one region (Leu328-Asp335) partly located in the pTyr recognition loop (Asn331-Cys338)(Barr et al. 2009; Zhang et al. 2012) might be changed, such as Asn331, Arg332, Tyr333, Gly334 and Asp335. We inferred that the compound **1h** would influence the function of this loop region, which could be one of the reasons for its inhibitory effect. It also could be seen that the whole fluctuations of PTP-MEG2/**1h** system was larger than that in the PTP-MEG2 system, indicating that the average atomic mobility of backbone atoms (N, C α and C) during MD simulation was increased in the PTP-MEG2/**1h** system. Therefore, the large fluctuations of whole system would change the

stability of conformations of PTP-MEG2/**1h**. The conformations needed for the catalytic activity could be no longer maintained. The results would be another reason for **1h** inhibitory effect.

To sum up, when the compound **1h** bound to the PTP-MEG2, the conformations of the protein became unstable, and thus, we speculated that the conformations needed for the catalytic activity might be no longer maintained due to the increased fluctuations of structure of the PTP-MEG2/**1h**. Meanwhile, the fluctuation of the the pTyr recognition loop (Asn331-Cys338) was decreased in the PTP-MEG2/**1h** system, inferring that the conformations of residues in this region might be changed and the interactions between residues in this region and residues in other regions might also be changed, therefore, it could be deduced that the catalytic activity might be directly influenced by the inhibitor **1h**. These results might be the way that inhibitor **1h** inhibited the PTP-MEG2.

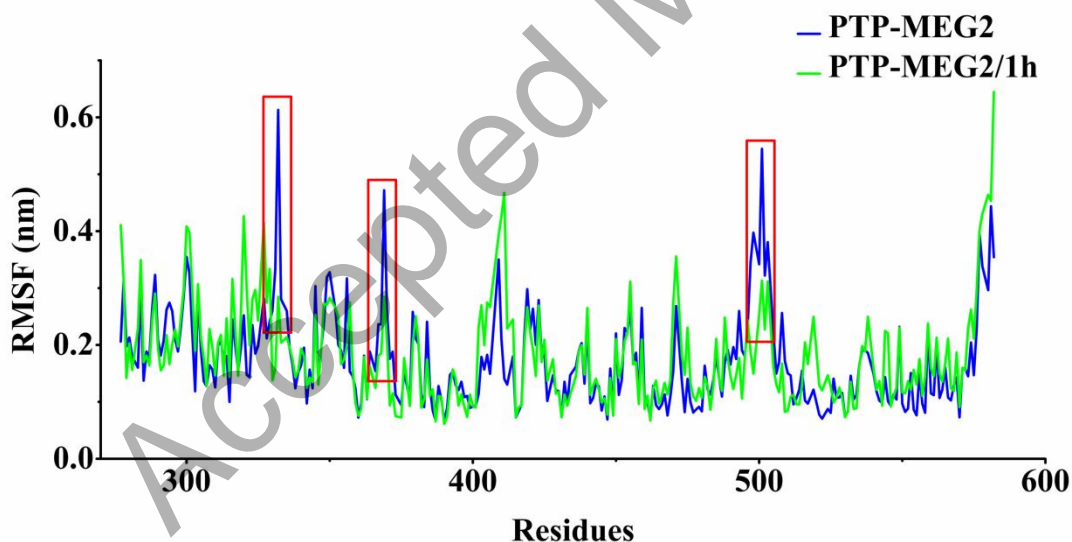


Figure 5 RMSF of the PTP-MEG2 system (blue line) and PTP-MEG2/**1h** system (green line) over 100 ns MD simulation. The red boxes represent the large differences between the two systems.

3.4.3 Principal component analysis (PCA)

To gain insight into the motions associated with conformation, we examined the conformational behavior of PTP-MEG2 system and PTP-MEG2/1h system by projecting them along the first three principal component or eigenvector (PC1, PC2 and PC3) directions.

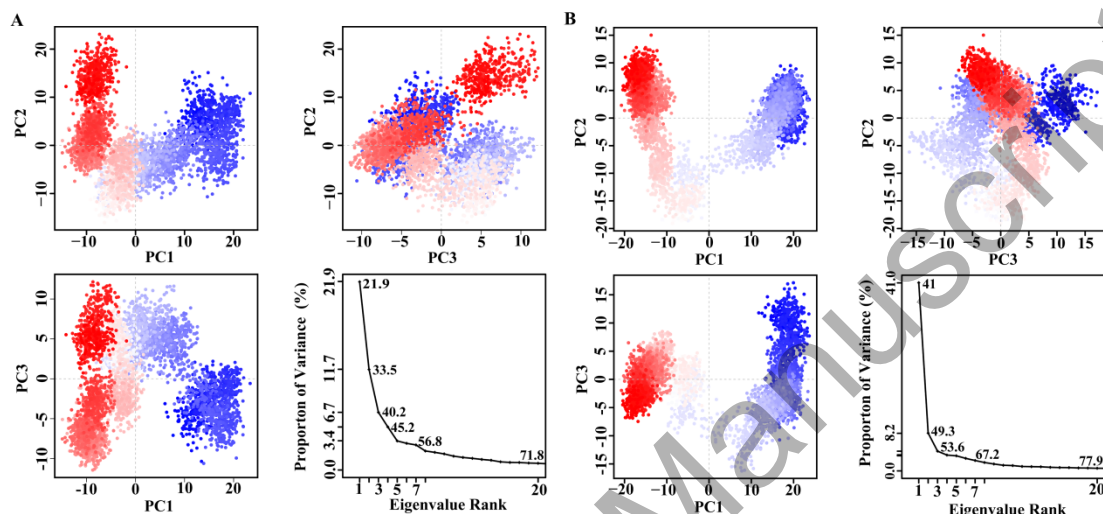


Figure 6. PCA scatter plots projecting principal components (PC1, PC2 and PC3) in the space of (A) PTP-MEG2 system and (B) PTP-MEG2/1h system.

As shown in the **Figure 6**, eigenvectors computed from the MD trajectories for the two systems were quite varied, displaying significant differences in motion across the three principal components, which clearly indicated the differences in protein motion and the conformational landscape between the PTP-MEG2 and the PTP-MEG2/1h. In the PTP-MEG2/1h system (**Figure 6B**), there were the highest correlated motion along PC1, PC2 and PC3 with a percentage of 41%, 8.3% and 4.3%, respectively, whereas in the PTP-MEG2 system (**Figure 6A**), the values of the three PCs were 21.9%, 11.6% and 6.7%, respectively, suggesting that the correlated motion was much more in the PTP-MEG2/1h system than in PTP-MEG2 system. Meanwhile, we could

also see from the scatter plot that there were much more the light red or blue dots in the PTP-MEG2/**1h** system than in the PTP-MEG2 system, indicating that the unstable conformations were increased in the PTP-MEG2/**1h** system due to the compound **1h**. The results showed that the PTP-MEG2/**1h** system was more flexible than the PTP-MEG2 system, which was agreed with the above RMSF, RMSD and Rg analyses.

3.4.4 Dynamics cross-correlation matrix (DCCM) analysis

To get a further insight of the conformational changes of PTP-MEG2 upon the compound **1h**, DCCM analysis was carried out to determine the presence of correlated motions. As shown in the **Figure 7**, the DCCM of the two systems was compared. The cyan and light cyan represented the positive correlated motions of residues, whereas the pink and light pink represented the anti-correlated movements of residues.

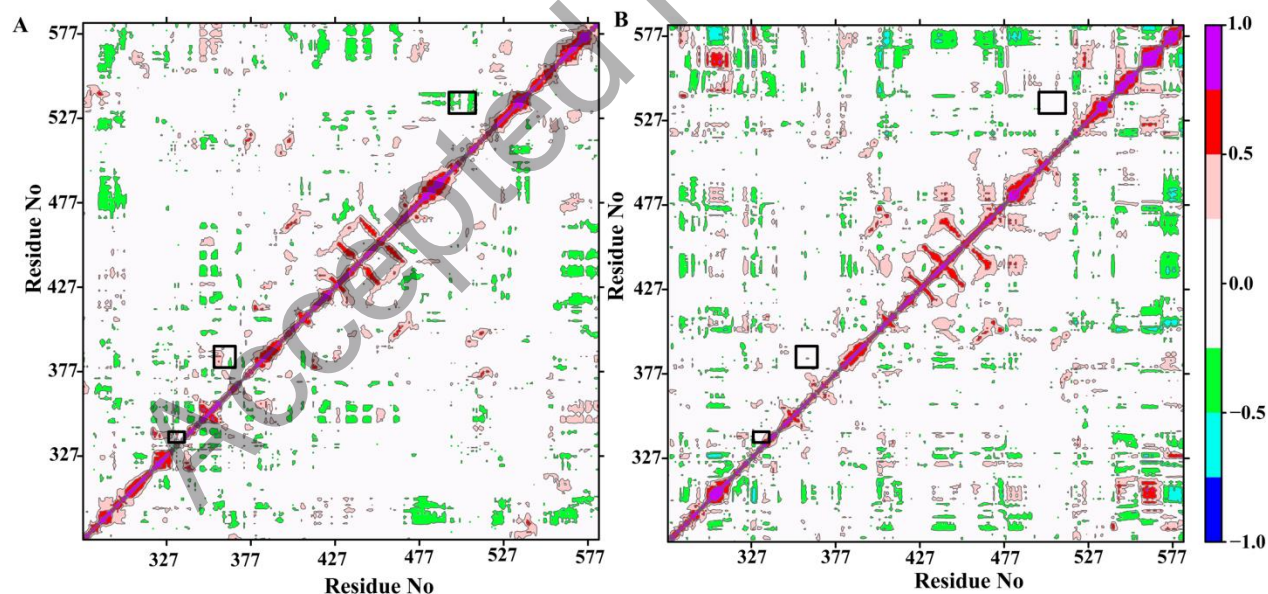


Figure 7. Cross-correlation matrices of the fluctuations of C- α atoms in PTP-MEG2 system (A) and PTP-MEG2/**1h** (B).

DCCM analysis showed that binding of **1h** changed the structure conformation of PTP-MEG2 as reflected in the correlated motions and dynamics. Firstly, it could be seen from the **Figure7** that the the positive correlated motions and the anti-correlated motions of residues were both increased in the PTP-MEG2/**1h** system, which indicated that fluctuations of the residues in the system was enhanced. Therefore, the stability of conformations of the PTP-MEG2/**1h** was decreased, which was agreed with the above analyses. Secondly, it could be also shown that the correlations of three regions marked by the blue boxes changed a lot when the compound **1h** bound to the protein. The positive correlated motions of residues between the region Leu328-Cys338 and Asp335-Asp340 were subdued, interestingly, we could infer that the fluctuations of residues in the pTyr recognition loop, such as Asn331, Arg332, Tyr333, Gly334, Asp335, Val336, Pro337 and Cys338 would be decreased due to the decreased correlations between this region and other region. Similarly, both the anti-correlated movements of residues between His352-Phe362 and Gly377-Asp385 and that between Val495-Pro507 and Ile530-Thr540 were also diminished, indicating that the correlations of these regions were reduced in the PTP-MEG2/**1h** system.

Thus, the fluctuations of these regions were decreased in this system, which was agreement with the RMSF analysis. In brief, DCCM analysis showed that the protein conformations became unstable and the fluctuation of pTyr recognition loop (Asn331-Cys338) was inhibited owing to the decreased correlations between this region and other region, which was agreement with the above analyses.

3.4.5 Residue interaction network analysis

To further explore the effect of the compound **1h** on the residues interactions in PTP-MEG2, the residue interaction network (RIN) analysis was performed. Firstly, the closeness centrality and shortest path betweenness of the residues were calculated by the tool of RINalyzer and NetworkAnalyzer in the Cytoscape. And thus, the notable residues in protein could be screened out, which could be utilized to reflect whether the protein system was stable or not. It could be seen from the table S1 that there were 10 notable residues, such as Cys567, Met550, Ser548, Asp529, Leu528, Phe525, Met400, Val399, Asp385 and Asn359 in the PTP-MEG2 system, whereas in the PTP-MEG2/**1h** system, the number of the notable residues was 7, and they were Met550, Phe525, Met400, Val399, Asp385, Asn359 and Arg332, respectively. We could find that the number of notable residues was decreased, which might cause the protein conformation unstable. Meanwhile, the Arg332 was found as notable residue, with the closeness centrality value 1.0 and shortest path betweenness value 0.1327. Secondly, the degree of the residues was calculated to further study the key residue. The three regions (Leu328-Asp335, Tyr366-Asn370 and Val495-Ser502) which showed large differences in above analysis were carried out to analyze. The table S2 showed that the Arg332 owned biggest changes, and the difference of it between PTP-MEG2/**1h** and PTP-MEG2 was 3. In brief, the Arg332 might be the key residues which would play an important role in disturbing the residue interaction. Furthermore, the detailed changes of the correlations in the above analyses were shown in **Figure 8**. The red dotted lines and the red rectangles represented the interactions and residues in the PTP-MEG2/**1h**, respectively, whereas the green dotted lines represented the interactions in the PTP-MEG2 system. The black dotted lines represented the interactions in both systems. Thus, we could find the Arg332 owned three interactions with Glu329, Leu379 and Leu328 in the PTP-MEG2/**1h** system, whereas in the PTP-MEG2 system it had only one interaction with Glu329. To sum up, we speculated that the Arg332 would be the key residues.

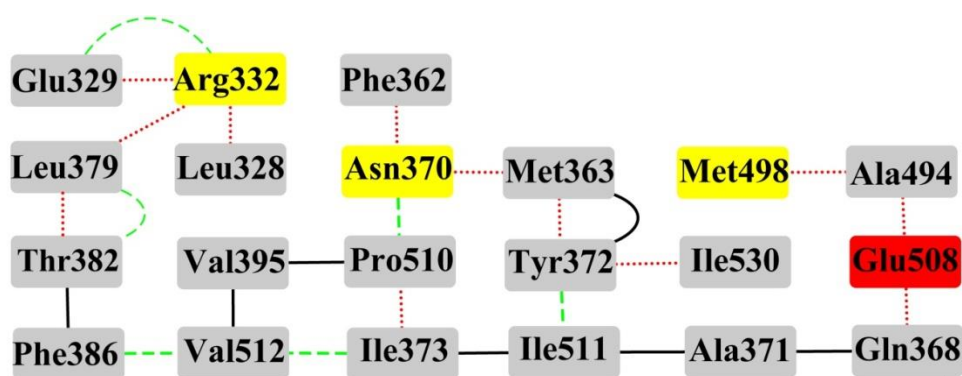


Figure 8 The residue interaction network analysis for the PTP-MEG2 and PTP-MEG2/**1h** systems. The red dotted lines and the red rectangles represented the interactions and residues in the PTP-MEG2/**1h**, respectively, whereas the green dotted lines represented the interactions in the PTP-MEG2 system. The black dotted lines represented the interactions in both systems.

4 Conclusions

In conclusion, a series of novel (R)-5-methylthiazolidin-4-one derivatives targeting PTP-MEG2 were designed with the aid of de novo design method. The designed compounds were synthesized, and their activities against PTP-MEG2 were evaluated. The results showed that the (R)-5-methylthiazolidin-4-one derivatives inhibited PTP-MEG2 within the micromolar range (1.34 μ M ~ 13.33 μ M). Compound **1h**, displaying the best inhibitory activity with an IC_{50} value of 1.34 μ M, was further validated by the method of molecular dynamics simulations. In this study, the various post-dynamics analyses were used to explore the effect of the compound **1h** on the PTP-MEG2, such as the RMSD, Rg, RMSF, PCA, DCCM and RIN analyses. The results suggested that when the compound **1h** bound to the PTP-MEG2, the protein conformations became unstable, indicating that the conformations needed for the catalytic activity was no longer maintained. Meanwhile, the fluctuations of the pTyr recognition loop (Asn331-Cys338) was increased in the PTP-MEG2/**1h** system, indicating that the conformations of this region might

also be changed, and thus, the function of catalytic activity site might be inhibited by the **1h**. This is exactly how the compound **1h** works, disturbing not only the pTyr recognition loop conformations, but also the protein conformations. Furthermore, we also found the key residues Arg332 would play an important role in disturbing the residue interactions.

Supporting Information.

The synthetic details of the desired products **1a-1h** and Tables (**Table S1** and **Table S2**) for residue interaction network analysis have been provided.

Acknowledgment

This work was supported by the National Natural Science Foundation of China (91773569), Natural Science Foundation of Tianjin (16JCZDJC32500 and 18JCQNJC13700) and Science & Technology Development Fund of Tianjin Education Commission for Higher Education (2017KJ229). Furthermore, we are grateful for Tianjin Key Laboratory on Technologies Enabling Development of Clinical Therapeutics and Diagnostics (Theranostics).

Conflict of Interest: The authors declare that they have no conflict of interest.

Reference

- Aier, I., Varadwaj, P. K. & Raj, U. (2016). Structural insights into conformational stability of both wild-type and mutant EZH2 receptor. *Scientific Reports* 6.
- Böhm, H.-J. (1992). The computer program LUDI: a new method for the de novo design of enzyme inhibitors. *Journal of Computer-Aided Molecular Design* 6: 61-78.
- Balmith, M. & Soliman, M. E. (2017). Non-active site mutations disturb the loop dynamics, dimerization, viral budding and egress of VP40 of the Ebola virus. *Mol Biosyst* 13: 585-597.
- Barr, A. J., Ugochukwu, E., Lee, W. H., King, O. N., Filippakopoulos, P., Alfano, I., Savitsky, P., Burgess-Brown, N. A., Muller, S. & Knapp, S. (2009). Large-scale structural analysis of the classical human protein tyrosine phosphatome. *Cell* 136: 352-363.
- Berhanu, W. M. & Masunov, A. E. (2014). Full length amylin oligomer aggregation: insights from molecular dynamics simulations and implications for design of aggregation inhibitors. *J Biomol Struct Dyn* 32: 1651-1669.

- Berman, H. M., Battistuz, T., Bhat, T., Bluhm, W. F., Bourne, P. E., Burkhardt, K., Feng, Z., Gilliland, G. L., Iype, L. & Jain, S. (2002). The protein data bank. *Acta Crystallographica Section D: Biological Crystallography* 58: 899-907.
- Buslaev, P., Gordeliy, V., Grudinin, S. & Gushchin, I. (2016). Principal Component Analysis of Lipid Molecule Conformational Changes in Molecular Dynamics Simulations. *J Chem Theory Comput* 12: 1019-1028.
- Chatterjee, S., Khunti, K. & Davies, M. J. (2017). Type 2 diabetes. *The Lancet* 389: 2239-2251.
- Cheng, X. C., Wang, R. L., Dong, Z. K., Li, J., Li, Y. Y. & Li, R. R. (2012). Design, synthesis and evaluation of novel metalloproteinase inhibitors based on L-tyrosine scaffold. *Bioorg Med Chem* 20: 5738-5744.
- Cho, C. Y., Koo, S.-H., Wang, Y., Callaway, S., Hedrick, S., Mak, P. A., Orth, A. P., Peters, E. C., Saez, E. & Montminy, M. (2006). Identification of the tyrosine phosphatase PTP-MEG2 as an antagonist of hepatic insulin signaling. *Cell Metabolism* 3: 367-378.
- Diller, D. J. & Merz Jr, K. M. (2001). High throughput docking for library design and library prioritization. *Proteins: Structure, Function, and Bioinformatics* 43: 113-124.
- Diller, D. J. & Merz, K. M. (2001). High throughput docking for library design and library prioritization. *Proteins: Structure, Function, and Bioinformatics* 43: 113-124.
- Fakhar, Z., Govender, T., Maguire, G. E. M., Lamichhane, G., Walker, R. C., Kruger, H. G. & Honarparvar, B. (2017). Differential flap dynamics in l,d-transpeptidase2 from mycobacterium tuberculosis revealed by molecular dynamics. *Mol Biosyst* 13: 1223-1234.
- Foster, C. A. & West, A. H. (2017). Use of restrained molecular dynamics to predict the conformations of phosphorylated receiver domains in two-component signaling systems. *Proteins* 85: 155-176.
- Gurzov, E. N., Stanley, W. J., Brodnicki, T. C. & Thomas, H. E. (2015). Protein tyrosine phosphatases: molecular switches in metabolism and diabetes. *Trends in Endocrinology and Metabolism* 26: 30-39.
- He, R., Zeng, L. F., He, Y., Zhang, S. & Zhang, Z. Y. (2013). Small molecule tools for functional interrogation of protein tyrosine phosphatases. *The FEBS journal* 280: 731-750.
- Hendriks, W., Bourgonje, A., Leenders, W. & Pulido, R. (2018). Proteinaceous regulators and inhibitors of protein tyrosine phosphatases. *Molecules* 23: 395.
- Hendriks, W. J., Elson, A., Harroch, S., Pulido, R., Stoker, A. & den Hertog, J. (2013). Protein tyrosine phosphatases in health and disease. *The FEBS journal* 280: 708-730.
- Huynh, H., Wang, X., Li, W., Bottini, N., Williams, S., Nika, K., Ishihara, H., Godzik, A. & Mustelin, T. (2003). Homotypic secretory vesicle fusion induced by the protein tyrosine phosphatase MEG2 depends on polyphosphoinositides in T cells. *The Journal of Immunology* 171: 6661-6671.
- Irwin, J. J. & Shoichet, B. K. (2005). ZINC— a free database of commercially available compounds for virtual screening. *Journal of Chemical Information and Modeling* 45: 177-182.
- Law, R., Barker, O., Barker, J. J., Hestekamp, T., Godemann, R., Andersen, O., Fryatt, T., Courtney, S., Hallett, D. & Whittaker, M. (2009). The multiple roles of computational chemistry in fragment-based drug design. *Journal of computer-aided molecular design* 23: 459-473.
- Lee, H., Yi, J.-S., Lawan, A., Min, K. & Bennett, A. M. (2015). *Mining the function of protein tyrosine phosphatases in health and disease*. Seminars in Cell & Developmental Biology, Elsevier.

- Li, H., Huang, J., Chen, L., Liu, X., Chen, T., Zhu, J., Lu, W., Shen, X., Li, J. & Hilgenfeld, R. (2009). Identification of novel falcipain-2 inhibitors as potential antimalarial agents through structure-based virtual screening. *Journal of medicinal chemistry* 52: 4936-4940.
- Li, H. L., Ma, Y., Zheng, C. J., Jin, W. Y., Liu, W. S. & Wang, R. L. (2018). Exploring the effect of D61G mutation on SHP2 cause gain of function activity by a molecular dynamics study. *J Biomol Struct Dyn* 36: 3856-3868.
- Liu, X., Dong, G., Zhang, J., Qi, J., Zheng, C., Zhou, Y., Zhu, J., Sheng, C. & , J. (2011). Discovery of novel human acrosin inhibitors by virtual screening. *Journal of computer-aided molecular design* 25: 977-985.
- Loving, K., Alberts, I. & Sherman, W. (2010). Computational approaches for fragment-based and de novo design. *Current Topics in Medicinal Chemistry* 10: 14-32.
- Lukman, S., Lane, D. P. & Verma, C. S. (2013). Mapping the structural and dynamical features of multiple p53 DNA binding domains: insights into loop 1 intrinsic dynamics. *PLoS One* 8: e80221.
- Ma, Y., Wang, S. Q., Xu, W. R., Wang, R. L. & Chou, K. C. (2012). Design novel dual agonists for treating type-2 diabetes by targeting peroxisome proliferator-activated receptors with core hopping approach. *PLoS One* 7: e38546.
- MacKerell, A. D., Bashford, D., Bellott, M., Dunbrack, R. L., Evanseck, J. D., Field, M. J., Fischer, S., Gao, J., Guo, H., Ha, S., Joseph-McCarthy, D., Kuchnir, L., Kuczera, K., Lau, F. T., Mattos, C., Michnick, S., Ngo, T., Nguyen, D. T., Prodhom, B., Reiher, W. E., Roux, B., Schlenkrich, M., Smith, J. C., Stote, R., Straub, J., Watanabe, M., Wiorkiewicz-Kuczera, J., Yin, D. & Karplus, M. (1998). All-atom empirical potential for molecular modeling and dynamics studies of proteins. *J Phys Chem B* 102: 3586-3616.
- Ndagi, U., Mhlongo, N. N. & Soliman, M. E. (2017). The impact of Thr91 mutation on c-Src resistance to UM-164: molecular dynamics study revealed a new opportunity for drug design. *Mol Biosyst* 13: 1157-1171.
- Niu, Y. Z., Shi, D. F., Li, L. L., Guo, J. Y., Liu, H. X. & Yao, X. J. (2017). Revealing inhibition difference between PFI-2 enantiomers against SETD7 by molecular dynamics simulations, binding free energy calculations and unbinding pathway analysis. *Scientific Reports* 7.
- Piovesan, D., Minervini, G. & Tosatto, S. C. (2016). The RING 2.0 web server for high quality residue interaction networks. *Nucleic Acids Res* 44: W367-374.
- Qi, Y., Zhao, R., Cao, H., Sui, X., Krantz, S. B. & Zhao, Z. J. (2002). Purification and characterization of protein tyrosine phosphatase PTP - MEG2. *Journal of Cellular Biochemistry* 86: 79-89.
- Shannon, P., Markiel, A., Ozier, O., Baliga, N. S., Wang, J. T., Ramage, D., Amin, N., Schwikowski, B. & Ideker, T. (2003). Cytoscape: A software environment for integrated models of biomolecular interaction networks. *Genome Research* 13: 2498-2504.
- Shoichet, B. K. (2004). Virtual screening of chemical libraries. *Nature* 432: 862-865.
- Sittel, F., Jain, A. & Stock, G. (2014). Principal component analysis of molecular dynamics: On the use of Cartesian vs. internal coordinates. *Journal of Chemical Physics* 141.
- Wang, D., Cheng, Z., Zhao, M., Jiao, C., Meng, Q., Pan, H., Xie, Y., Li, L., Zhu, Y. & Wang, W. (2019). PTPN9 induces cell apoptosis by mitigating the activation of Stat3 and acts as a tumor suppressor in colorectal cancer. *Cancer management and research* 11: 1309.
- Wu, J.-w., Yin, L., Liu, Y.-q., Zhang, H., Xie, Y.-f., Wang, R.-l. & Zhao, G.-l. (2019). Synthesis, biological evaluation and 3D-QSAR studies of 1, 2, 4-triazole-5-substituted carboxylic

- acid bioisosteres as uric acid transporter 1 (URAT1) inhibitors for the treatment of hyperuricemia associated with gout. *Bioorganic & Medicinal Chemistry Letters* 29: 383-388.
- Wu, J.-W., Zhang, H., Duan, Y.-Q., Dong, W.-L., Cheng, X.-C., Wang, S.-Q. & Wang, R.-L. (2014). Design novel inhibitors for treating cancer by targeting Cdc25B catalytic domain with de novo design. *Combinatorial Chemistry & High Throughput Screening* 17: 837-847.
- Zhang, L. S., Wang, S. Q., Xu, W. R., Wang, R. L. & Wang, J. F. (2012). Scaffold-based pan-agonist design for the PPARalpha, PPARbeta and PPARgamma receptors. *PLoS One* 7: e48453.
- Zhang, S., Chen, L., Luo, Y., Gunawan, A., Lawrence, D. S. & Zhang, Z.-Y. (2009). Acquisition of a potent and selective TC-PTP inhibitor via a stepwise fluorophore-tagged combinatorial synthesis and screening strategy. *Journal of the American Chemical Society* 131: 13072-13079.
- Zhang, S., Liu, S., Tao, R., Wei, D., Chen, L., Shen, W., Yu, Z. H., Wang, L., Jones, D. R., Dong, X. C. & Zhang, Z. Y. (2012). A highly selective and potent PTP-MEG2 inhibitor with therapeutic potential for type 2 diabetes. *J Am Chem Soc* 134: 18116-18124.
- Zhang, X., Wu, J., Liu, Y., Xie, Y., Liu, C., Wang, J. & Zhao, G. (2017). Facile synthetic approaches to 1-thiocyclopropanecarboxylates. *Phosphorus, Sulfur, and Silicon and the Related Elements* 192: 799-811.
- Zhang, Z.-Y. (2001). Protein tyrosine phosphatases: prospects for therapeutics. *Current Opinion in Chemical Biology* 5: 416-423.